

Equally Distributing Points on the Complex Plane to Measure the Complex Reflectivity of an Optical Cavity

Deedee Jansen¹ and Todd Kozloeski²

¹Department of Physics, Austin College, Sherman, Texas

¹Deutsches Elektronen-Synchrotron DESY, Notkestr. 85, 22607
Hamburg, Germany

August 2024

1 Abstract

In this study, we investigate a method for accurately measuring the complex reflectivity of an optical cavity using heterodyne interferometry. Our approach focuses on the distribution of measurement points on the complex plane to optimize the precision and accuracy of cavity characterization. We demonstrate the limitations of equally spaced frequency points, which result in uneven data density across critical regions such as resonance. To address this, we employ a non-equally spaced frequency sampling technique that ensures a uniform distribution of points on the complex plane, particularly around the free spectral range (*FSR*). This method provides a more precise analysis of the cavity's complex reflectivity, transmissivity, and optical losses.

2 Introduction

Heterodyne interferometry uses a probe field's phase and amplitude to characterize the optical cavity's complex reflectivity. Optical cavities are used in gravitational wave detection, dark matter candidate searches, vacuum magnetic birefringence detection, and precision tests of quantum geometry at the Planck scale. Heterodyne interferometry can be used to characterize these cavities independently of the calibration of the photodetectors. This occurs when a probe and local oscillator fields are injected into the cavity at opposite mirrors.

In a Fabry-Perot cavity with two mirrors, M_1 and M_2 , with reflection and transmission coefficients r_1 and t_1 , and r_2 and t_2 . Then, for each mirror, the reflectivity R , transmissivity T , and excess optical losses L , can be represented in terms of power.

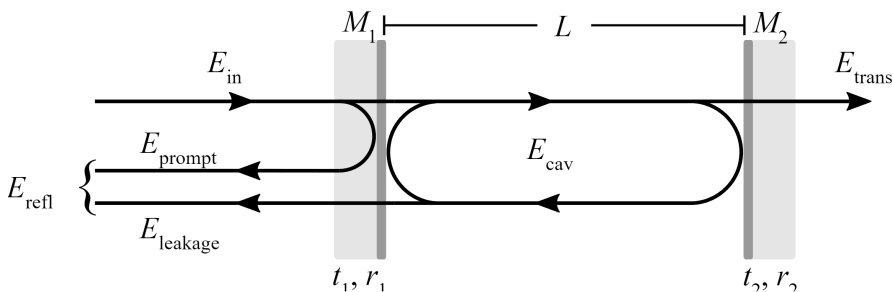


Figure 1: Schematic of a Fabry-Perot optical cavity with two mirrors, M_1 and M_2 , illustrating the electric fields involved in characterizing the cavity's reflectivity and transmissivity using heterodyne interferometry. Here, E_{in} is the incident electric field, E_{refl} is the reflected electric field, E_{prompt} is the prompt reflection, $E_{leakage}$ is the leakage field through the input mirror, E_{cav} is the circulating field inside the cavity, and E_{trans} is the transmitted electric field. The reflection and transmission coefficients for mirrors M_1 and M_2 are r_1 , t_1 and r_2 , t_2 , respectively.

$$R_{1,2} = |r_{1,2}|^2 \quad (1)$$

$$T_{1,2} = |t_{1,2}|^2 \quad (2)$$

So by the conservation of energy

$$R + T + L = 1 \quad (3)$$

Understanding the phase difference between the incident and reflected electric fields in a Fabry-Perot optical cavity is essential for characterizing the cavity's behavior. Figure 2 illustrates how the phase difference between E_{refl} and E_{in} can be graphically represented.

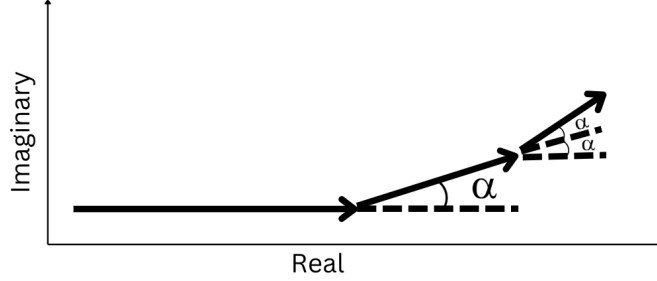


Figure 2: Phase relationships in an optical cavity: The phase difference α the field inside the cavity of the E_{refl} and the incident electric field E_{in} in a Fabry-Perot cavity, the offset compounds each trip the light makes through the cavity.

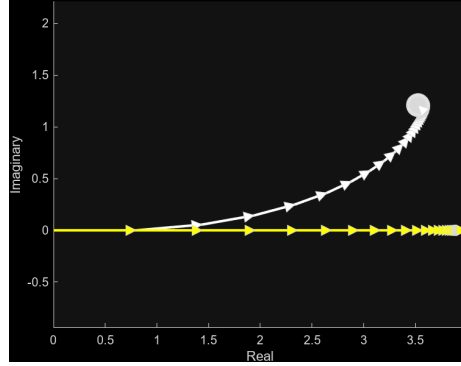


Figure 3: The convergence of the vectors illustrates the stabilization of the phase difference, which is crucial for determining the cavity's complex reflectivity. Convergence in this context refers to the sum of the (decreasingly sized) vectors. This stability is essential for accurately characterizing the cavity's behavior, including its reflectivity and transmissivity.

The circle traced out by the the cavity complex field for a given round trip phase detuning α of various phase differences can be drawn in the complex plane. This circle can be represented by the equation for complex reflectivity, derived from when perfect mode matching is achieved. This occurs when the incident light's spatial profile matches the cavity's eigenmodes. With perfect mode matching between the input field and the cavity, the reflected field is the reflected input field, $r_1 E_i$, and the field leaks through the input mirror, $t_1 r_2 e^{ikl} E_{cav}$. The field can be understood to be

$$E_{ref} = r_1 E_i - t_1 r_2 e^{ikl} E_{cav} \quad (4)$$

Where E_i is the monochromatic laser field coupled into the cavity by M_1 . And

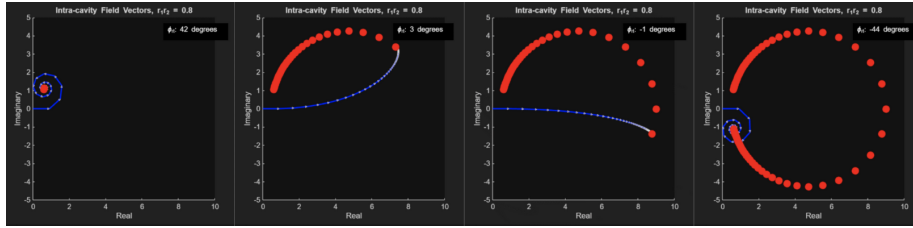


Figure 4: Intra-cavity Field Vectors: The phase difference ϕ_{it} at various degrees (42° , 3° , -1° , -44°) showing the trajectories of intra-cavity field vectors in the complex plane. As ϕ changes a circle in the complex plane is traced out.

$E_{cav} = t_1 E_i / (1 - r_1 r_2 e^{ikl})$. The Cavity is on resonance and has its maximum circulating field when kl is an integer multiple of 2π , which happens when the round-trip optical path length of the cavity is an integer multiple of λ .

The transmitter leakage is a phase shift of π from the reflected field. So the E_{ref} becomes

$$E_{ref} = E_i (r_1 - t_1 r_2 e^{ikl} / (1 - r_1 r_2 e^{ikl})) \quad (5)$$

The cavity complex reflectivity, \mathcal{R} , is the ratio of the reflected and incident fields; with a high-finesse cavity near resonance, it can be approximated as

$$\mathcal{R}(\Delta\nu) = E_{ref} / E_i \approx 1 - T_1 / (A/2 - i\Delta\nu/f_0) \quad (6)$$

Where $A = T_1 + L_1 + T_2 + L_2$ is the total attenuation of the circulating power during a single cavity round-trip, $\Delta\nu$ is the frequency difference between the input laser field and the nearest cavity resonance, and f_0 is the cavity-free spectral range. (Spector and Kozlowski, 2024)

These two equations can be represented on the complex plane. As the frequency difference between the lase and the cavity resonance $\Delta\nu$ is scanned, a circle is formed in the complex plane. Here, the circle's diameter ratio to the distance from the origin to its future point is $2T_1/A$ (Spector and Kozlowski, 2024). Scanning the input field frequency relative to the cavity resonance allows the arc of the circle traced out to be measured, as can A , T_1 , and FSR .

Heterodyne interferometry is used to measure this complex reflectivity. This is done by coupling a local oscillator (LO) laser into the cavity and then interfering with the probe field in reflection with the LO in transmission. When this is done, only the portion of the probe field's light, which is in the spatial mode of the cavity, contributes to the beat-note amplitude and phase. (Spector and Kozlowski, 2024)

Prior use of this technique employed equally spaced frequency points. When these points are graphed in the complex plane, it results in a higher density of points at the ends of the frequency range and fewer points around the free spectral range (FSR). This uneven distribution can be problematic because it leads to insufficient data around critical regions such as the resonance, where more detailed information is crucial for accurate analysis.

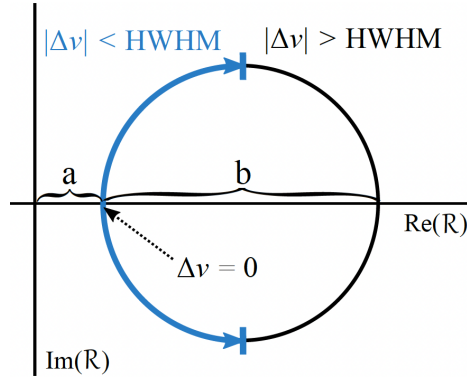


Figure 5: Illustration of the field reflected on the complex plane. As the frequency $\Delta\nu$ is sweeping, the $R(\Delta\nu)$ traces out this circle, where the diameter $b/(a+b)$ can be used to find $2T_1/A$. The blue section is the frequency within the cavity with, and $a+b$ gives the amplitude of the input field E_i (Spector and Kozłowski, 2024)

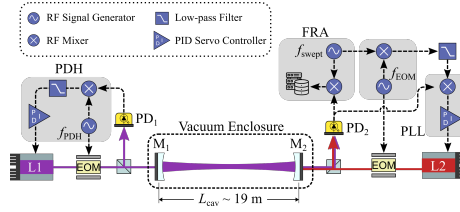


Figure 6: This is a Schematic Layout of the Experiment, where Laser 1 serves as the resonant local oscillator and Laser 2 generates the probe field, which gives the cavity complex reflectivity from the side of Laser 2 and, therefore, T_2 . To get the T_1 , the control loops are switched. Spector and Kozłowski, 2024

Using equally spaced frequency points means the spacing between each measured frequency is constant. While this approach can simplify data collection, it fails to account for the non-linear response around the resonance frequency. In the complex plane plot, this manifests as a clustering of points near the extremities of the range and sparse coverage near the resonance. Such an uneven distribution can lead to less accurately representing the resonance characteristics. By analyzing the complex reflectivity, we can infer the transmissivity and optical losses, providing a comprehensive understanding of the material's interaction with light. This understanding is crucial for optimizing material performance in optical applications, where precise control over reflectivity and transmission can significantly improve device efficiency and functionality.

This paper is structured as follows: Section 2 outlines the experimental setup and methodologies used for measuring the refractive index and extinction coefficient across the specified spectral range. Section 3 presents the data

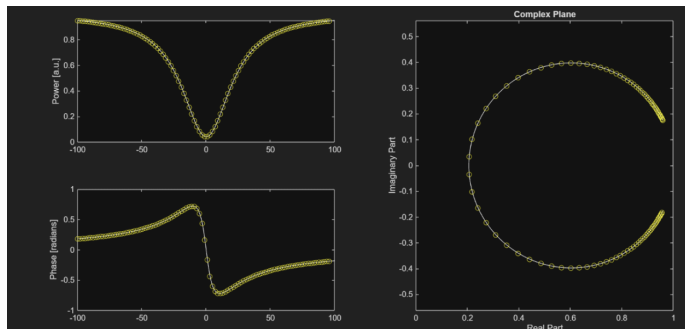


Figure 7: Frequency Response Analysis Using Equally Spaced Frequency Points This image illustrates the results of a frequency response analysis where the measurement points were equally spaced apart in frequency. The diagrams showcase: Power vs. Frequency Plot (Top Left): This plot displays the signal’s power as a function of frequency, with a distinct dip at the cavity’s resonance frequency. Phase vs. Frequency Plot (Bottom Left): This plot shows the signal’s shift across the same frequency range, highlighting the phase transition at resonance. Complex Plane Plot (Right): Plots the real and imaginary parts of the signal in the complex plane, demonstrating the distribution of points around the resonance.

analysis techniques employed to derive complex reflectivity from the measured parameters. Section 4 discusses the results, focusing on the relationship between complex reflectivity, transmissivity, and optical losses. Finally, Section 5 concludes the paper by summarizing the key findings and their implications for developing and optimizing optical materials.

3 Procedure

3.1 The Cavity

The 19-meter-long cavity used to run this experiment used a 50.8mm diameter with a radius of curvature of 19.95m mirrors from *LaserOptik GmbH*. They were coated with alternating silica/tantalum dielectric layers deposited on a polished fused silica substrate. The mirror mount is controlled via piezo actuators, allowing for adjustments under vacuum. (Spector and Kozlowski, 2024)

A free spectral range (FSR) of 7.89160 ± 0.00001 MHz was measured, giving a single-pass optical path length of 18.99440 ± 0.00002 m.

3.2 Distribution of Points

Our study found that points distributed evenly along the frequency would not be even in the complex plane. This challenge is similar to what Baity et al. (2024) described in their work on optimizing the circle fit for resonant quality

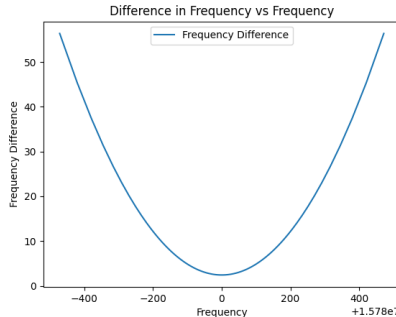


Figure 8: This graph shows the difference between the frequencies being measured. It is the lowest and centered around the FSR, where the most data is going to be taken.

measurements in superconducting resonators, where they developed equations to find the frequency to measure such that the points in the complex plain were equally distributed. Baity et al., 2024

We adopted the approach of Baity et al., utilizing their foundational equations as a basis for our analysis. However, to tailor their model for superconducting resonators to optical resonators, we put their equations in terms of our known variables (Baity et al., 2024)

$$\theta(f) = 2 \arctan(2(FSR/FSR)(1 - f/FSR)) \quad (7)$$

$$f(\theta) = FSR - FWHM/2 * \tan(\Theta/2) \quad (8)$$

We then set the frequency to $\pm 500 FSR$. This allowed us to create an array of frequencies centered around the FSR , with most measurements taken close to it.

3.3 Measurement Technique

A Moku Pro, made by Liquid Instruments Instruments, 2024, was used in multi-instrument mode to string together two lock-in amplifiers and a laser lock box to measure heterodyne cavity reflectivity.

Our experiment used the Pound-Drever-Hall (PDH) laser frequency stabilization technique to precisely characterize an optical cavity. The process involved two lasers: a resonant local oscillator (LO) laser, which was locked to the cavity using PDH, and an auxiliary probe laser, whose frequency was scanned over a cavity resonance.

The implementation of the PDH technique within this scheme involved several steps. First, Laser 1 (LO) was locked to the cavity using PDH (Black, 2001). This required modulating the phase of Laser 1 with an electro-optic modulator

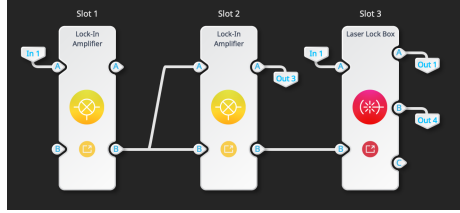


Figure 9: The connections of the Moku Pro in Multi-Instrument Mode . The lock-in amplifier in slot one acts as a frequency response analyzer where the list of frequencies is sent in. The laser lock box keeps the pound driver hall lock.

(EOM) and detecting the reflected light from the cavity. The reflected signal was mixed with the modulation signal to produce an error signal, which was then used to give feedback to Laser 1’s frequency, locking it to the cavity resonance. Next, Laser 2 (Probe) was stabilized relative to Laser 1 through an offset phase-locked loop (PLL), ensuring the probe laser remained off-resonance during the measurement. This maintained PLL stability and preserved phase information. Subsequently, Laser 2 was phase-modulated to generate sidebands, with the upper sideband used as the probe. The frequency of this probe sideband was then swept across a cavity resonance. Finally, the probe field reflected from the cavity interfered with the LO field transmitted through the cavity in a heterodyne detection setup. This ensured that only the portion of the probe field spatially matched to the cavity’s fundamental mode contributed to the beat note, whose amplitude and phase were measured as the probe frequency was scanned (Spector and Kozlowski, 2024).

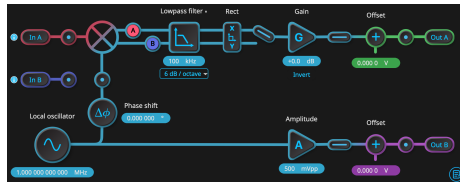


Figure 10: This diagram depicts the setup of the first lock-in amplifier configured as a frequency response analyzer. Key components and their functions are illustrated as follows: Local Oscillator: This generator generates the frequencies that define the frequency of the probe field relative to resonance, resulting in a complex reflectivity encoded in the amplitude and phase of the beat note. Measurement Points (A and B): Points where the in-phase (I) and quadrature (Q) signals are measured, providing crucial data on the cavity’s reflectivity.

The first Lock-in Amplifier, which worked as a Frequency Response Analyzer, scanned the frequency. The array of frequencies was fed into the locking amplifier’s local oscillator, which gave the cavity its complex reflectivity, as it

was encoded in the amplitude and phase of the beat note. The Q and I signals were measured at points A and B in Figure 10. The get data function in the Moku python API was used to collect 1024 points over one second; this was then averaged to find the average Q and I signals for each frequency measured.

3.4 Data Processing

In our analysis, the processing of collected data involved several key steps, particularly fitting a circle to the measured Q and I data points and calculating the residual sum of squares (RSS) to evaluate the fit quality. These steps are essential for accurately characterizing our system's frequency response and ensuring that our measurements are reliable and precise.

The initial data collection was performed by sweeping the frequency and recording the corresponding I and Q signals. These signals were then used to calculate the amplitude and phase of the response at each frequency point.

$$Amplitude = \sqrt{I^2 + Q^2} \quad (9)$$

$$Phase = \arctan[Q/I] \quad (10)$$

The collected data was unwrapped to ensure continuity in the phase measurements, adjusted by subtracting the average phase to normalize the data.

We applied a circle-fitting algorithm to analyze the I and Q data. This method is crucial for identifying the resonance characteristics in the complex plane. The circle fitting was performed using the following linear algebra approach:

We set up the system of linear equations based on the geometric relationship of the data points (x_i, y_i) to the circle's center (c_x, c_y) and the radius R .

$$(x_i - c_x)^2 + (y_i - c_y)^2 = r^2 \quad (11)$$

This can be rearranged into a linear form to facilitate the use of linear least squares fitting

$$x_i^2 + y_i^2 = 2c_x x_i + 2c_y y_i + r^2 - c_x^2 - c_y^2 \quad (12)$$

In matrix form, this can be written as:

$$\begin{bmatrix} x_1 & y_1 & 1 \\ x_2 & y_2 & 1 \\ \cdot & \cdot & \cdot \\ \cdot & \cdot & \cdot \\ \cdot & \cdot & \cdot \\ x_n & y_n & 1 \end{bmatrix} \begin{bmatrix} 2c_x \\ 2c_y \\ r^2 - c_x^2 - c_y^2 \end{bmatrix} = \begin{bmatrix} x_1^2 + y_1^2 \\ x_2^2 + y_2^2 \\ \cdot \\ \cdot \\ \cdot \\ x_n^2 + y_n^2 \end{bmatrix} \quad (13)$$

Solving this system using least squares gives the values of c_x , c_y , and $r^2 - c_x^2 - c_y^2$. The radius r can then be calculated.

The residual sum of squares (RSS) is calculated to assess the fit's quality. This measures the difference between the distances of the data points from the fitted circle and the radius.

$$RSS = \sum (\sqrt{(x_i - c_x)^2 + (y_i - c_y)^2} - r)^2 \quad (14)$$

4 Results

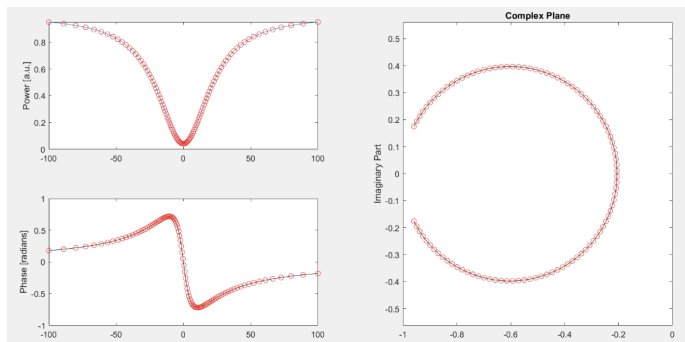


Figure 11: This image presents the results of a frequency response analysis where the measurement points were non-equally spaced in frequency but rather equally spaced around the complex plane, specifically designed to provide denser coverage around the resonance. The diagrams display: Power vs. Frequency Plot (Top Left): This plot shows the signal’s power as a function of frequency, with a clear dip at the cavity’s resonance frequency. Phase vs. Frequency Plot (Bottom Left): This plot illustrates the signal’s phase shift across the frequency range, highlighting the phase transition at resonance. Complex Plane Plot (Right): This plot depicts the real and imaginary parts of the signal in the complex plane, showing a more uniform distribution of points around the resonance.

In the preceding analysis, we utilized equally spaced frequency points, resulting in an uneven data distribution in the complex plane. We implemented a non-equally spaced frequency sampling technique to address this issue, concentrating more points around the free spectral range (FSR) and resonance regions.

The results, as shown in the accompanying figure 11, demonstrate several improvements: The power and phase plots now exhibit a more refined and continuous transition at the resonance. The increased data density around the critical regions ensures that the key features of the resonance are captured more accurately. The complex plane plot displays a uniform distribution of points around the resonance. This balanced coverage enhances the precision of the frequency response characterization.

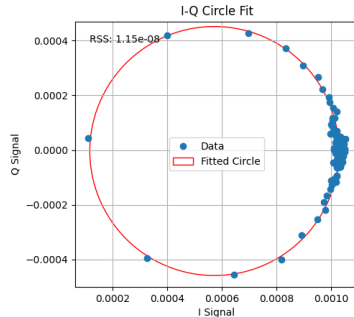


Figure 12: Initial distribution of signal data points in the Q-I plane, including the fitted circle and the calculated residual sum of squares (RSS) value. The higher RSS indicates a less accurate fit, demonstrating the initial alignment and spread of the data points around the circle.

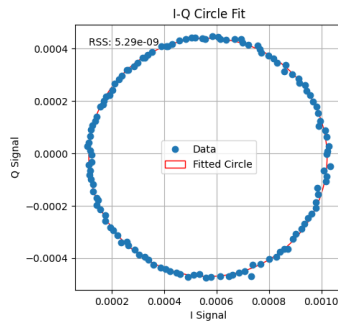


Figure 13: After applying the proposed technique, the distribution of signal data points in the Q-I plane was enhanced. The fitted circle shows a significantly lower residual sum of squares (RSS) value, indicating an improved fit and demonstrating the technique’s effectiveness in refining data alignment.

To evaluate the performance of our signal processing technique, we analyzed the distribution of data points in the Q-I plane (Quadrature and In-phase components). The results are illustrated in Figures 12 and 13 . Figure 12 shows the initial distribution of the signal data points, the fitted circle, and the calculated residual sum of squares (RSS) value. Similarly, Figure 13 presents the distribution after applying the improved technique.

The circle-fitting technique involves plotting the data points in the Q-I plane and fitting a circle to these points. The RSS value determines the goodness of fit, with a lower RSS indicating a better fit. The primary aim is to achieve a uniform distribution of the data points around the fitted circle, which signifies a stable and consistent signal representation. Initially, the RSS value was significantly

higher, at $1.15\text{e-}8$, indicating a less accurate fit. This is evident in the spread and alignment of the data points with respect to the fitted circle. After applying our refined technique, the RSS value was notably reduced to $5.26\text{e-}9$, indicating a much better fit. The data points aligned more closely with the fitted circle, suggesting a more uniform distribution.

5 Discussion

The results of our study demonstrate that non-equally spaced frequency sampling provides a significant advantage over equally spaced frequency points, particularly in measuring the complex reflectivity of an optical cavity.

Concentrating more points around the resonance ensures the critical regions are more densely sampled. This results in a more accurate and detailed representation of the resonance characteristics in both the power and phase plots.

The significant reduction in the RSS value after applying the non-equally spaced frequency sampling strategy indicates a better fit of the circle to the data points. This improvement underscores the effectiveness of the proposed technique in refining the alignment of data points and enhancing measurement accuracy.

A significant benefit of fitting a circle to the complex plane plot is that it allows us to extract critical optical properties such as transmittance, losses, and reflectivity. Equally spaced frequency points often result in uneven distributions in the complex plane, particularly at resonance frequencies. The inherent non-linear response of optical cavities around resonance means that points concentrated at extremities provide limited insight into the cavity's behavior near resonance. This uneven distribution can lead to inaccuracies in characterizing the cavity's reflectivity and transmissivity, as critical resonance features may not be captured adequately. The circle fit helps to accurately determine the complex reflectivity, which lets us find the reflectivity, transmissivity, and optical losses.

The improved circle fit in the complex plane evidences the effectiveness of our method. Compared to equally spaced frequency measurements, our approach reduced the residual sum of squares (RSS) and enhanced the accuracy of the fitted circle. Overall, our findings highlight the importance of optimizing the distribution of measurement points in frequency response analysis. The proposed non-equally spaced frequency sampling strategy offers a robust approach for achieving more precise and reliable characterization of optical cavities.

6 Conclusion

The experiment successfully demonstrated the application of heterodyne interferometry in measuring the complex reflectivity of an optical cavity by evenly distributing frequency measurement points in the complex plane. This approach overcame the limitations of traditional equally spaced frequency measurements, leading to improved data density around critical resonance regions and more

accurate characterization of the cavity’s properties.

In the initial setup, the distribution of signal data points in the complex plane exhibited noticeable deviations from the ideal circular pattern, reflecting inaccuracies in our frequency response measurements. Figure 13 shows the data points’ initial alignment and the fitted circle, with a relatively high residual sum of squares (RSS) indicating a less accurate fit. However, after applying the proposed non-equally spaced frequency sampling technique, the distribution of data points in the complex plane was significantly enhanced. Figure 14 illustrates this improvement, with a fitted circle showing a substantially lower RSS value. This indicates a much more accurate fit and demonstrates the technique’s effectiveness in refining data alignment and improving the overall precision of the frequency response analysis.

We effectively increased data density around the resonance by adopting a method that ensures points are evenly distributed in the complex plane. This approach facilitated more accurate calculations of the complex reflectivity $R(\Delta\nu)$, allowing us to better understand the optical cavity’s behavior. The evenly spaced points provided a more balanced view of the cavity’s response, accurately capturing the phase and amplitude variations.

The technique Baity et al. (2024) developed was instrumental in our analysis, offering a way to determine the frequency points needed for even distribution in the complex plane. We adapted their equations to suit the context of optical cavities, focusing on critical variables such as the free spectral range (FSR) and full width at half maximum ($FWHM$). Our method centered around the FSR , allowing for finer measurements near resonance, where the cavity’s behavior is most sensitive. (Baity et al., 2024)

The comparison between the initial and enhanced distributions shows that our optimized sampling strategy leads to more reliable and accurate measurements, providing a robust basis for characterizing the optical cavity’s complex reflectivity and transmissivity, successfully demonstrating an improved method for characterizing the complex reflectivity of an optical cavity using heterodyne interferometry. By adopting a non-equally spaced frequency sampling strategy, we achieved a more uniform distribution of data points in the complex plane, particularly around the resonance regions. This led to more accurate and reliable measurements, as evidenced by the reduced RSS values and enhanced data alignment in the complex plane.

The next phase of this research will focus on refining the measurement parameters to further enhance the accuracy and reliability of our optical cavity characterizations. Specifically, we will experiment with different sampling densities around the resonance frequency and explore adaptive techniques that dynamically adjust the frequency points based on initial measurements. This optimization aims to reduce measurement time while maintaining or improving the precision of the reflectivity and transmissivity calculations. Additionally, we will conduct out-of-loop experiments to validate the accuracy of our complex reflectivity measurements. This approach will use independent measurement systems to assess and compare the cavity’s response with our current findings. By ensuring consistency between in-loop and out-of-loop measurements, we can

confirm the reliability of our method and identify potential sources of error or bias in the current setup. We plan to extend our measurements over multiple free spectral ranges (FSR) to comprehensively understand the cavity’s behavior. This broader range will allow us to identify phase offsets potentially introduced by physical wiring and other systematic errors. By analyzing the cavity’s response across a more comprehensive frequency range, we can detect anomalies and refine our setup to ensure accurate phase alignment and minimize external influences on the measurements.

Our findings underscore the importance of optimizing frequency sampling techniques in interferometric measurements, particularly when precise characterization of optical cavities is required. The proposed approach can significantly benefit various advanced applications, including gravitational wave detection, dark matter searches, and high-resolution spectroscopy, where accurate cavity characterization is crucial.

7 Acknowledgments

I sincerely thank the University of Florida for the International Research Experience for Undergraduates opportunity. Special thanks to Dr. Paul Fulda, Dr. Peter Wass, and Dr. Sujda Krishna for their invaluable guidance. I am also grateful for the assistance of the ALPS group at DESY a, particularly Arron Spector and the Optics team. I sincerely thank Todd Kozlowski for his significant contributions and mentorship. I also want to extend my appreciation to my IREU cohort for their camaraderie. This work was funded by the National Science Foundation under grant NSFPHY-2348913.

References

- Baity, P. G., Maclean, C., Seferai, V., Bronstein, J., Shu, Y., Hemakumara, T., & Weides, M. (2024). Circle fit optimization for resonator quality factor measurements: Point redistribution for maximal accuracy. *Physical Review Research*, 6(1), 013329.
- Black, E. D. (2001). An introduction to pound-drever-hall laser frequency stabilization. *American Journal of Physics*, 69(1), 79–87.
- Instruments, L. (2024). Moku:pro with 14+ integrated instruments [Accessed: 2024-08-01].
- Spector, A. D., & Kozlowski, T. (2024, April). Optical cavity characterization with a mode-matched heterodyne sensing scheme.